Analysis of Three-Dimensional Ducted and Exhaust Plume Flowfields

Sanford M. Dash*
Aeronautical Research Associates of Princeton, Inc., Princeton, N.J.
and
Paul D. DelGuidice†
Grumman Aerospace Corporation, Bethpage, N.Y.

Computational procedures are described for analyzing three-dimensional supersonic internal flows and multinozzle exhaust plume flowfields. The computer codes (BIGMAC and CHAR3D) embodying these procedures cater to a broad spectrum of geometric situations via the use of multiple reference plane grid networks in several coordinate systems. Shock capturing techniques are employed to trace the propagation and interaction of multiple shock surfaces. Gas properties consist of combustion products in chemical equilibrium. The computational accuracy of the codes is assessed via comparisons with the results of other codes and experimental data. Results are presented for the flows in two-dimensional ducts, corner flows, flow in a rectangular nozzle, and the plume flowfields for exhausts issuing out of single and multiple rectangular nozzles.

Introduction

COMPUTATIONAL models have been developed for analyzing the complex inviscid supersonic flowfields within three-dimensional ducts of arbitrary geometry and the exhaust plume flowfields associated with generalized multiple nozzle configurations. The flowfields specifically considered in the development of these models are those associated with airbreathing hypersonic aircraft, such as the typical integrated nozzle configuration depicted in Fig. 1 which is characterized by multiple rectangular nozzle modules. A dominant feature of such nozzle/exhaust flows is the presence of multiple interacting shock surfaces. Shock waves are produced in the vicinity of the injectors, and the flowfield within the individual modules involves complex shock interactions with waves generated and reflected from mutually perpendicular surfaces. Downstream of the nozzle exit plane, the underexpanded exhaust plumes from the individual modules interact with the nonuniform vehicle external flowfield resulting in an expansion system propagating toward the vehicle undersurface from the cowl trailing edge and a spanwise expansion generated by the sidewall interaction. A plume-generated bow shock propagates into the external flow and a spanwise multiple shock system occurs due to the mismatch in pressure and flow deflection between adjacent modules.

To accommodate the analysis of rather arbitrary geometric configurations, a reference plane approach has been utilized in which the three-dimensional volume under consideration is spanned by several groups of appropriately selected coordinate planes in several different coordinate systems. The equations of motion within the reference planes are expressed in a quasistreamline coordinate system (quasistreamlines are the projections of the actual stream surfaces onto these reference planes) catering to the calculation of rotational variable-composition flowfields and chosen for ease in including the effects of transport processes normal to the streamlines and finite-rate chemistry along the streamlines in subsequent phases of this effort.

Submitted Oct. 3, 1977; revision received April 26, 1978.

Index categories: Computational Methods; Supersonic and Hypersonic Flow; Nozzle and Channel Flow.

*Consultant. Member AIAA.
†Senior Research Scientist.

The reference plane approach in conjunction with a quasicharacteristic numerical procedure has been widely used in analyzing supersonic flows around generalized bodies.[1-3] The authors have previously developed a model[4,5] in which this procedure was extended to analyze three-dimensional nozzle/exhaust flowfields. In this model, the dominant discontinuity surfaces such as the plume bow shock and interface were analyzed discretely; but, no special treatment of secondary shocks was provided for leading to results of unacceptable quality in situations involving multiple shock interactions.

Whereas the conclusion had been reached[6] that finite-difference codes are better able to analyze complex multishocked flows than reference plane characteristic (refchar) codes, the authors demonstrated[7] that poorer performance of refchar codes was largely due to the inverse interpolation procedures employed. As such, a parallel effort was undertaken to develop both characteristic (CHAR3D) and finite-difference (BIGMAC) reference plane codes in which the accurate analysis of secondary shock processes would be of prime concern. CHAR3D employs a novel wave-preserving network in conjunction with a nonisentropic pressure-density relation to achieve shock-capturing capabilities, whereas BIGMAC makes use of conservation variables in conjunction with a one-sided difference algorithm. While the numerical procedures employed in CHAR3D and BIGMAC differ, both codes employ the same geometry package[8] for a description of boundary contours, calculate all boundary points by reference plane characteristic procedures, and incorporate the same thermodynamic fits[5] for describing the hydrogen-air gas mixture in chemical equilibrium. Many other features in the authors' original refchar code[4,5] have been retained and improved upon in the current models.

A preliminary assessment of BIGMAC and CHAR3D in analyzing internal flows[7] showed both models to be capable of accurately predicting multiple shock interactions in two-dimensional situations. CHAR3D appeared well suited for analyzing flows where the predominant wave propagation occurred within the reference planes, yielding results comparable to those of BIGMAC and eliminating the overshoot in the vicinity of the shock associated with most finite-difference procedures. However, for flows with strong discontinuities propagating normal to the reference planes, CHAR3D produced results significantly inferior to those of BIGMAC.

Attempts to remedy this situation by using conservative one-sided differencing in evaluating the cross-flow derivative forcing function terms did not improve its performance significantly. Thus, only BIGMAC was extended to analyze the exhaust plume flowfield downstream of the engine modules which is characterized by large spanwise gradients and cross-flow shocks.

This paper will present a brief overview of the computational methodology employed in both BIGMAC and CHAR3D, concentrating upon the extensions of BIGMAC to the analysis of exhaust plume flows. Results are presented demonstrating the shock-capturing capabilities for flows within the reference planes and for flows in the vicinity of internal corners. Fully three-dimensional results are presented for the flow in a rectangular nozzle and in the exhaust plumes issuing from single and multiple rectangular nozzles. A more comprehensive description of both BIGMAC and CHAR3D, including additional results and comparisons, may be found in Refs. 9 and 10.

CHAR3D

The modified continuity and the three momentum equations in general orthogonal coordinates may be written

Modified Continuity:

$$\rho a^2\left(\frac{u_{x1}}{h_1}+\frac{w_{x3}}{h_3}\right)+\frac{uP_{x1}}{h_1}+\frac{wP_{x3}}{h_3}=\frac{-a^2}{h_1h_2h_3}\left[h_1h_3\left(\frac{v}{a^2}P_{x_2}+\rho v_{x_2}\right)+h_{2_{x_1}}h_3\rho u+h_1h_{2_{x_3}}\rho w\right] \tag{1}$$

x_1 Momentum:

$$\frac{u}{h_1}u_{x_1}+\frac{w}{h_3}u_{x_3}+\frac{1}{\rho h_1}P_{x_1}=-\frac{v}{h_2}u_{x_2}+\frac{v^2}{h_1h_2}h_{2_{x_1}} \tag{2}$$

x_2 Momentum:

$$\frac{u}{h_1}v_{x_1}+\frac{w}{h_3}v_{x_3}+\frac{1}{\rho h_2}P_{x_2}=-\frac{v}{h_2}v_{x_2}-\frac{uv}{h_1h_2}h_{2_{x_1}}-\frac{vw}{h_2h_3}h_{2_{x_3}} \tag{3}$$

x_3 Momentum:

$$\frac{u}{h_1}w_{x_1}+\frac{w}{h_3}w_{x_3}+\frac{1}{\rho h_3}P_{x_3}=-\frac{v}{h_2}w_{x_2}+\frac{v^2}{h_2h_3}h_{2_{x_3}} \tag{4}$$

Here, u, v, and w are the velocity components in the x_1, x_2, and x_3 directions; P is the pressure; ρ is the density; and a is the sound speed. The identification of metric coefficients, h_i, and coordinate directions for the three systems presently incorporated in the developed codes is provided in Table 1. Note that h_{2x_1} is unity for the line source system and zero for other systems while h_{2x_3} is unity for the cylindrical system and zero for other systems. These terms will be replaced by the indices J_1 and J_2, where $J_1=1$ for the line source system and $J_2=1$ for the cylindrical system. Both indices are zero otherwise. In writing Eqs. (1-4), the source terms and terms involving derivatives normal to the reference planes $x_2=$ constant have been put on the right-hand side. Then, the left-hand side of these equations corresponds to that of the two-dimensional system in the x_1, x_3 plane. Reference plane characteristic relations are readily obtained by algebraic manipulation of the modified continuity equation and the x_1 and x_3 momentum equations. These relations are listed below, where the velocity vector

$$\bar{V}=u\hat{i}_{x_1}+v\hat{i}_{x_2}+w\hat{i}_{x_3}$$

Table 1 Metric coefficients and coordinate directions

System	x_1	x_2	x_3	h_1	h_2	h_3
Cartesian	x	y	z	1	1	1
Cylindrical	x	θ	r	1	r	1
Line source	r	θ	z	1	r	1

is expressed in terms of its magnitude in the reference plane q, quasistreamline angle ϕ, and cross-flow angle ψ (Fig. 2), employing the geometric relations

$$q=(u^2+w^2)^{1/2} \tag{5a}$$

$$\phi=\tan^{-1}(w/u) \tag{5b}$$

$$\psi=\tan^{-1}(v/q) \tag{5c}$$

Along the reference plane characteristics

$$\lambda^{\pm}=\frac{dx_3}{dx_1}=\frac{M^2\cos\phi\sin\phi\pm\beta}{M^2\cos^2(\phi-1)} \tag{6}$$

the compatibility relations may be written

$$d\phi\pm(\beta/\Gamma M^2)\,d(\ell n\,P)=F^{\pm}\,d\bar{x} \tag{7}$$

where

$$F^{\pm}=(\sin\phi-\lambda^{\pm}\cos\phi)[(\tan\psi)_{x_2}+(\tan\psi/\Gamma)(\ell n\,P)_{x_2}]-\phi_{x_2}\tan\psi(\cos\phi+\lambda^{\pm}\sin\phi)+(J_2-\lambda^{\pm}J_1)\tan^2\psi$$

and

$$d\bar{x}=\frac{dx_1}{x_1^{J_1}x_3^{J_2}}$$

The streamline projections onto the reference planes

$$\lambda_{SL}=\frac{dx_3}{dx_1}=\tan\phi \tag{8}$$

are also characteristic directions for this system. Along the quasistreamline, λ_{SL}, a relation between ψ and P may be written:

$$d(\tan\psi)-(\tan\psi/\Gamma M^2)\,d(\ell n\,P)=G\,d\bar{x} \tag{9}$$

where

$$G=\frac{-1}{\cos\phi}\left[\frac{(\ell n\,P)_{x2}}{\Gamma M^2}+\tan\psi(\tan\psi)_{x_2}+\tan\psi(1+\tan^2\psi)(J_1\cos\phi+J_2\sin\phi)\right]$$

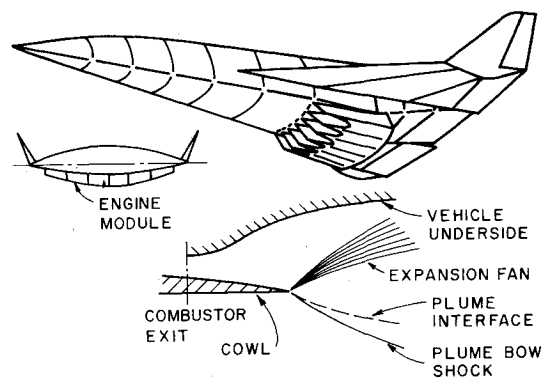

Fig. 1 Airbreathing aircraft integrated nozzle configuration.

The above relations are supplemented by expressions for the constancy of total enthalpy H, fuel-to-air ratio Φ, and entropy S, (in continuous regions of the flow) along streamlines. Curve fits for the isentropic exponent, $\Gamma=\Gamma(h,P,\Phi)$, for a hydrogen-air system are detailed in Refs. 5 and 9.

BIGMAC

The conservative form of the inviscid flow equations may be written

$$\bar{E}_{x_1}+\bar{F}_{x_2}+\bar{G}_{x_3}+\bar{H}=0 \tag{10}$$

where, for $k=1$ to 6,

$$\bar{E}(k)=h_2h_3\begin{bmatrix}\rho u\\ P+\rho u^2\\ \rho uv\\ \rho uw\\ \rho uH\\ \rho u\Phi\end{bmatrix} \qquad \bar{F}(k)=h_1h_3\begin{bmatrix}\rho v\\ \rho uv\\ P+\rho v^2\\ \rho vw\\ \rho vH\\ \rho v\Phi\end{bmatrix}$$

$$\bar{G}(k)=h_1h_2\begin{bmatrix}\rho w\\ \rho uw\\ \rho vw\\ P+\rho w^2\\ \rho wH\\ \rho w\Phi\end{bmatrix} \qquad \bar{H}(k)=\begin{bmatrix}0\\ -J_1h_3(P+\rho v^2)\\ (J_1h_3u+J_2h_1w)\rho v\\ -J_2h_1(P+\rho v^2)\\ 0\\ 0\end{bmatrix}$$

In performing the numerical integration of this system of equations, the same number of quasistreamlines are followed in each reference plane (in contiguous flow regions), and a one-to-one correspondence is made between similarly indexed streamlines in adjacent reference planes. Then Eq. (10) may be written

$$\bar{E}_{\tilde{x}_1}+\bar{F}_{\tilde{x}_2}+\bar{G}_{x_3}+\bar{H}-\frac{h_1}{h_3}\frac{w}{u}\bar{E}_{x_3}-\tan\alpha\frac{h_2}{h_3}\bar{F}_{x_3}=0 \tag{11}$$

where $\partial/\partial\tilde{x}_1$ denotes the partial derivative in the x_1 direction along the quasistreamline in the reference plane $x_2=$ constant, while $\partial/\partial\tilde{x}_2$ denotes the partial derivative in the x_2 direction along the line connecting "corresponding" streamline points on adjacent reference planes at the marching station $x_1=$ constant. Thus,

$$\left(\frac{\partial}{\partial x_1}\right)_{x_2,x_3}=\left(\frac{\partial}{\partial\tilde{x}_1}\right)_{x_2,\eta}-\frac{h_1}{h_3}\frac{w}{u}\left(\frac{\partial}{\partial x_3}\right)_{x_1,x_3}$$

and

$$\left(\frac{\partial}{\partial x_2}\right)_{x_1,x_3}=\left(\frac{\partial}{\partial\tilde{x}_2}\right)_{x_1,\xi}-\frac{h_2}{h_3}\tan\alpha\left(\frac{\partial}{\partial x_3}\right)_{x_1,x_3}$$

where $\tan\alpha$ is the angle made by the line connecting "corresponding" grid points in adjacent reference planes with respect to the x_2 coordinate direction, as illustrated in Fig. 2.

Computational Procedure

Both CHAR3D and BIGMAC employ analogous reference plane networks whose orientation for various configurations is documented in Refs. 5 and 9. The characteristic lattice in the reference plane utilized for CHAR3D (Fig. 3) differs from

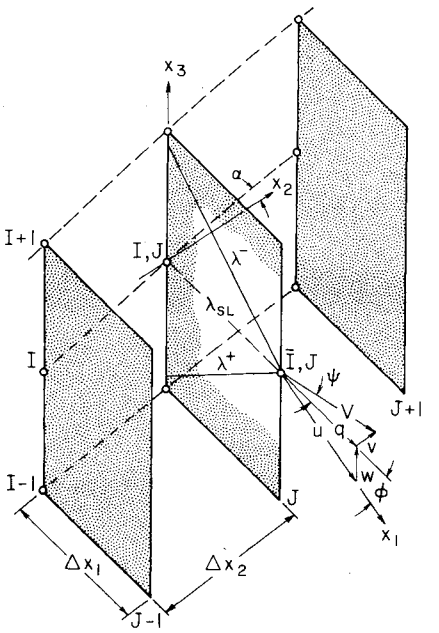

Fig. 2 Reference plane geometric nomenclature.

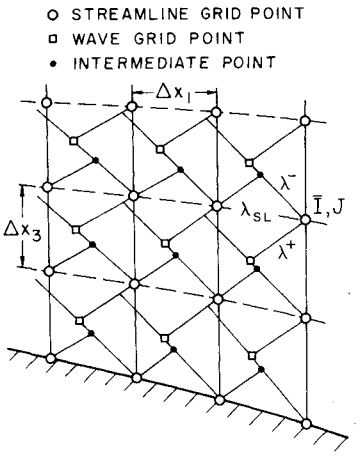

Fig. 3 CHAR3D grid lattice in the reference plane.

that of previous methods.[2-5] These employ a standard inverse scheme wherein interpolations are performed along a non-characteristic initial data surface thus ignoring information contained along already calculated quasicharacteristic surfaces. The use of the grid lattice in Fig. 3 in conjunction with linear interpolations along the quasicharacteristics has led to a marked improvement over inverse methods in describing wave processes in the reference planes.[7]

To obtain sufficient resolution in analyzing complex flowfields with multiple wave interactions, a highly refined computational grid may be required. This is provided for in BIGMAC and CHAR3D via the sequential calculation of limited portions of the flow in conjunction with disk transfer operations. In BIGMAC, for each marching step, a series of reference planes are calculated at a time, with the calculation proceedings from the lower to upper bounding surface in each reference plane. After the first block of calculations are completed, the results are stored on disk and the next block of reference plane data is read from disk and calculated. In CHAR3D, the procedure is performed in the opposite manner. Storage is allocated for several levels of data for all reference planes. Thus, the lower boundary points are first calculated by sweeping across all reference planes, yielding a quasicharacteristic surface for the calculation of the next

point up from the lower boundary. This process is continued to the upper bounding surface.

Interior Point Calculation

In CHAR3D, a somewhat complex procedure is entailed in determining properties at the point $\bar{I},J$ (Fig. 3) whose details may be found in Refs. 7, 9, and 10. In addition to the standard streamline grid points, an additional array of wave grid point data is required in the performance of this calculation. Difference expressions of the compatibility relations [Eq. (7)] along the reference plane characteristics $\lambda^{\pm}$, yield P and ϕ while ψ, Φ, H, and S are determined from difference expressions applied along the quasistreamlines λ_{SL}. The velocity is determined from the relation

$$V=[2H-2h(P,\Phi,T)]^{1/2}$$

in conjunction with the three parameter curve fits

$$h=h(P,\Phi,T) \qquad \rho=\rho(P,\Phi,T) \qquad \Gamma=\Gamma(P,\Phi,T)$$

detailed in Refs. 5 and 9. In the integration procedure, coefficient and forcing function terms are evaluated at the initial stations in the predictor step and averaged along the characteristics ($\lambda^{\pm}$ or λ_{SL}) in the corrector step. In regions of rapid change, several additional iterations may be required to ensure convergence.

In the vicinity of shock waves, the resultant entropy change, ΔS, is accounted for in the pressure-density relation applied along streamlines [i.e., for a perfect gas $\bar{V}\cdot\nabla \ell n\,(P/\rho^{\gamma})=\bar{V}\cdot\nabla S/C_v$]. ΔS is directly relatable to the shock strength ξ, via the (perfect gas) relation

$$\frac{\Delta S}{C_v}=\ell n\,\xi-\gamma\,\ell n\left[\frac{(\gamma+1)\xi+(\gamma-1)}{(\gamma-1)\xi+(\gamma+1)}\right] \tag{12}$$

Since the captured shock is generally spread over several Δx_I intervals ($K=1$ to K_f), the entropy change in the interval $K-1$ to K is given by

$$\left(\frac{\Delta S}{C_v}\right)_{K-1,K}=\ell n\left[\frac{\xi_{I,K}}{\xi_{I,K-1}}\frac{F(\xi_{I,K-1})}{F(\xi_{I,K})}\right]^{\gamma} \tag{13}$$

where $\xi_{I,K}=P_K/P_I$ and $F(\xi)$ is the bracketed term in Eq. (12). Since the shock geometry does not appear in the above entropy relation, entropy changes associated with complex three-dimensional shocks can be readily estimated. Special provisions[7,9,10] have been incorporated into CHAR3D to avoid singularities at multiple shock junctures and wall reflection points.

BIGMAC calculates interior points via the two-step MacCormack[11] algorithm applied to Eq. (11). In the predictor step

$$\tilde{E}_{\bar{I},J}=E_{I,J}-2\Delta x_I\left(F_{x_2}+G_{x_3}-\frac{h_I}{h_3}\frac{w}{u}E_{x_3}-\frac{h_2}{h_3}F_{x_3}\tan\alpha+\frac{H}{2}\right)_{I,J} \tag{14a}$$

while in the corrector step

$$E_{\bar{I},J}=\frac{1}{2}\left\{(\tilde{E}_{\bar{I},J}+E_{I,J})-2\Delta x_I\left[\tilde{F}_{x_2}+\tilde{G}_{x_3}-\frac{h_I}{h_3}\left(\frac{\tilde{w}}{u}\right)\tilde{E}_{x_3}-\frac{h_2}{h_3}\tilde{F}_{x_3}\tan\tilde{\alpha}+\frac{\tilde{H}}{2}\right]_{\bar{I},J}\right\} \tag{14b}$$

where, for the vector array V,

$$(V_{x_2})_{I,J}=\pm\left(\frac{V_{I,J\pm1}-V_{I,J}}{d_I+d_2}\right)\left(\frac{d_I}{d_2}\right)^{\pm1}$$

$$(V_{x_3})_{I,J}=\pm\left(\frac{V_{I\pm1,J}-V_{I,J}}{d_3+d_4}\right)\left(\frac{d_3}{d_4}\right)^{\pm1}$$

and

$$d_I=x_{2_{I,J}}-x_{2_{I,J-1}}$$

$$d_2=x_{2_{I,J+1}}-x_{2_{I,J}}$$

$$d_3=x_{3_{I,J}}-x_{3_{I-1,J}}$$

$$d_4=x_{3_{I+1,J}}-x_{3_{I,J}}$$

Physical variables are obtained by standard uncoupling procedures.

Wall Point Calculation

Surface geometry is prescribed via discrete contour data for all continuous surfaces comprising the nozzle/afterbody configuration. Thus, for analyzing rectangular modules, as depicted in Fig. 1, contour data are provided for the sidewalls, vehicle undersurface, and cowl. Surface "fitting" is done by program FIT3D[8] which generates ordered surface coefficient arrays to be employed in BIGMAC and CHAR3D in conjunction with surface interpolation procedures.[8,9]

Both CHAR3D and BIGMAC employ reference plane characteristic procedures in the performance of *all* boundary calculations. In CHAR3D, the finite-difference expressions for the characteristic compatibility relation [Eq. (7)] and cross-flow momentum equation [Eq. (9)], along with the relation expressing $\bar{V}\cdot\hat{n}=0$ in the coordinate system of interest, yield three nonlinear equations from which the values of P, ϕ, and ψ at the boundary point can be extracted via a simple iterative procedure. In BIGMAC, a linear system of difference equations in $\ell n\,P$, (w/u), and (v/u) is obtained, which for a surface given by $x_3=f(x_1,x_2)$ may be written:

$$\begin{bmatrix}(\rho u^2/\beta P)_{\lambda^{\pm}} & \pm 1 & 0\\ 1 & 0 & -(f_{x_2})_c/h_2\\ (vw/q^2)_{\lambda_{SL}} & (v/u\cdot P/\rho q^2)_{\lambda_{SL}} & -1\end{bmatrix}\times\begin{bmatrix}(w/u)_c\\ \ell n\,P_c\\ (v/u)_c\end{bmatrix}=\begin{bmatrix}R_1\\ R_2\\ R_3\end{bmatrix} \tag{15}$$

where the R_i involve cross-derivative and forcing function terms.[7,9,10]

In CHAR3D, the entropy changes associated with shocks produced at, or reflected from, solid boundaries is obtained by the procedure outlined in the previous section. Rather than incorporate this complex methodology in BIGMAC, it has proven effective to set the entropy change along the wall equal to that along the streamline one-mesh interval away from the wall.

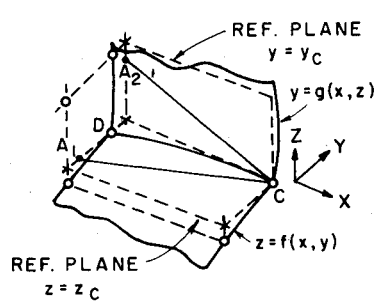

Fig. 4 Internal corner point.

Corner Point Calculation

Internal corners, as at the juncture of the sidewalls with the cowl or vehicle undersurface, are analyzed in both codes by a redundant "weighted" characteristic procedure. The boundary condition $\bar{V}\cdot\hat{n}=0$ applied at the corner to intersecting surfaces of the form $z=f(x,y)$ and $y=g(x,z)$ (Fig. 4) yields the expressions

$$\frac{w}{u}=\tan\phi=\frac{f_x+g_xf_y}{1-g_zf_y} \tag{16a}$$

and

$$\frac{v}{q}=\tan\psi=\cos\phi\frac{g_x+f_xg_z}{1-f_yg_z} \tag{16b}$$

for the flow deflection angles ϕ and ψ. Application of characteristic compatibility relations along A_2C and A_1C in the reference planes $y=y_c$ and $z=z_c$ both yield values of the corner point pressure P_C. A weighting of these pressures accounting for the relative wave strengths in both reference planes is performed using the relation

$$P_C=\frac{\Delta\psi_{A_1C}}{\Delta\psi_{A_1C}+\Delta\phi_{A_2C}}P_{C_1}+\frac{\Delta\phi_{A_2C}}{\Delta\psi_{A_1C}+\Delta\phi_{A_2C}}P_{C_2} \tag{17}$$

while streamline relations applied along the corner, *CD*, yield remaining flowfield variables.

Surfaces of Discontinuity

The predominant discontinuity surfaces, such as the plume interface separating the exhaust and external flows and the plume-induced external shock, are discretely analyzed. The computational procedures developed have been implemented in the authors' original code[4,5]; but, at present, only the plume interface methodology has been incorporated into BIGMAC. These procedures are detailed in Refs. 5 and 9 and briefly summarized herein.

In the reference plane approach, local surface orientation (Fig. 5) is readily specified by an orthonormal triad of vectors comprised of the unit normal $\hat{n}$, a tangent vector $\hat{t}$ (with cosine director β) in the reference plane $x_2=$constant, and the tangent vector $\hat{\ell}$ (with cosine director α) given by $\hat{n}=\hat{t}\times\hat{\ell}$. The unit normal $\hat{n}$, expressed in terms of α and β, is given by

$$\hat{n}=-\cos\alpha\sin\beta\hat{i}_{x_1}-\sin\alpha\,\hat{i}_{x_2}+\cos\alpha\cos\beta\hat{i}_{x_3} \tag{18}$$

where the cross-cut angle α' (made by the cut of the discontinuity surface with the plane $x_1=$constant with respect to the x_2 coordinate direction) is related to the angles α and β by $\tan\alpha'=\tan\alpha/\cos\beta$. Computations are performed in each reference plane assuming the cross-cut angle α' does not vary in the integration step, with the proper surface orientation then determined by iteratively varying β. Upon global convergence, values of α' are evaluated at the new station and the entire process is repeated using these new values.

For a shock point calculation, the relations to be satisfied in the $\hat{n}$, $\hat{t}$, and $\hat{\ell}$ directions are

$$\rho_1u_{n_1}(u_{n_1}-u_{n_2})=P_2-P_1 \tag{19a}$$

$$q_1\cos(\beta-\phi_1)=q_2\cos(\beta-\phi_2) \tag{19b}$$

$$q_1[-\sin\alpha\sin(\beta-\phi_1)+\cos\alpha\tan\psi_1]$$
$$=q_2[-\sin\alpha\sin(\beta-\phi_2)+\cos\alpha\tan\psi_2] \tag{19c}$$

where

$$u_n=q[\tan\psi\sin\alpha+\cos\alpha\sin(\beta-\phi)]$$

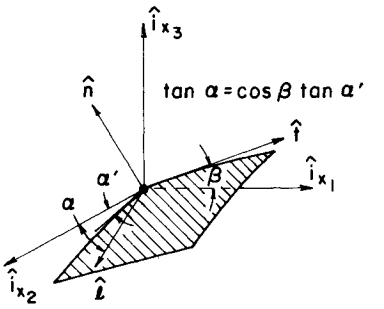

Fig. 5 Discontinuity surface orientation.

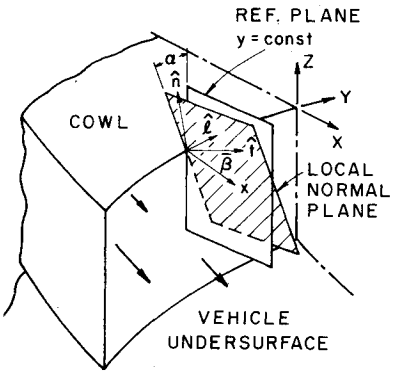

Fig. 6 Local normal plane for trailing edge interaction.

These relations are supplemented by the characteristic compatibility relation on the downstream side of the shock.

The plume interface calculation is substantially more complex than its two-dimensional counterpart since streamlines on either side not only differ in composition and stagnation properties, but also may be highly skewed with respect to each other. For the interface point calculation, a local iterative procedure is performed in each reference plane to satisfy the relations $\bar{V}_1\cdot\hat{n}=\bar{V}_2\cdot\hat{n}=0$ and $P_1=P_2$. The $\bar{V}\cdot\hat{n}$ relations in terms of α and β take the form

$$\sin(\beta-\phi_{1,2})+\tan\alpha\tan\psi_{1,2}=0 \tag{20}$$

and are supplemented by compatibility and streamline relations on either side of the interface.

Exit Plane Exhaust/External Flow Interaction

At the exit plane, the inviscid interaction between the nozzle exhaust flow and external stream is discretely analyzed establishing the initial geometry of the plume interface separating these streams. The calculation of this interaction is considerably simplified by recognizing that the flow phenomenon is locally two-dimensional in planes normal to the cowl trailing edge. Working in this coordinate system (Fig. 6), standard two-dimensional procedures are employed in determining the initial interface angle $\bar{\beta}$, which yields a pressure balance. For a nonswept trailing edge, the local unit vectors are obtained via the transformation

$$\begin{bmatrix}\hat{n}\\ \hat{\ell}\\ \hat{t}\end{bmatrix}=\begin{bmatrix}\sin\bar{\beta} & -\cos\bar{\beta}\sin\alpha & \cos\bar{\beta}\cos\alpha\\ 0 & \cos\alpha & \sin\alpha\\ \cos\bar{\beta} & -\sin\bar{\beta}\sin\alpha & \sin\bar{\beta}\cos\alpha\end{bmatrix}\begin{bmatrix}\hat{i}_{x_1}\\ \hat{i}_{x_2}\\ \hat{i}_{x_3}\end{bmatrix} \tag{21}$$

where $\hat{\ell}$ is the unit vector tangent to the cowl trailing edge and $\hat{n}$ is normal to the discontinuity surface at the trailing edge. The angle α is the cross-cut angle made by the cowl trailing edge with the x_2 coordinate direction, while β is an angle made by the cut of the discontinuity surface with the reference plane $x_2=$constant. The angle $\bar{\beta}$ is the cut of this discontinuity surface with the local normal plane and is related to α and β by the expression $\tan\bar{\beta}=\cos\alpha\tan\beta$.

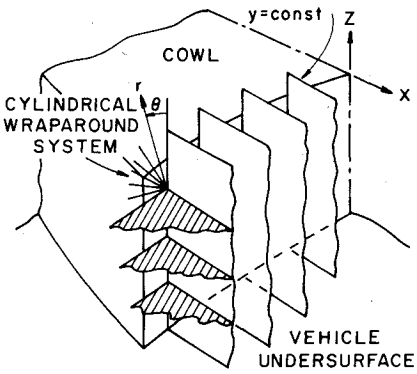

Fig. 7 Reference plane orientation in external corner region.

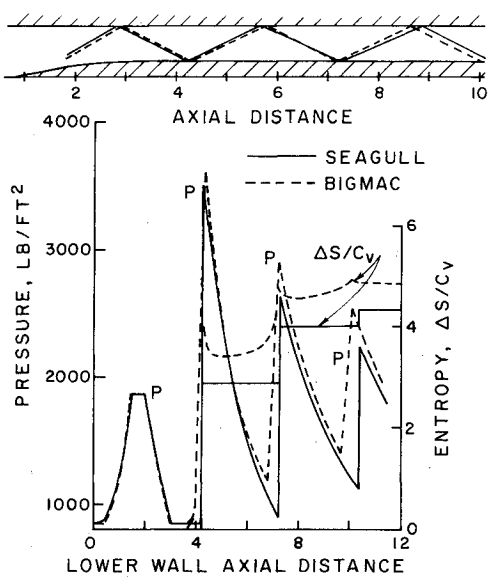

Fig. 8 Convergent duct calculation.

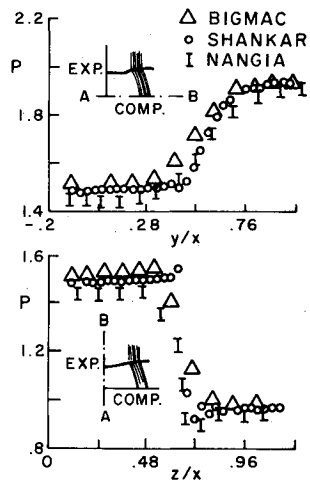

Fig. 9 Expansion-compression corner calculation.

External Corner Region

For an end module, the wave systems introduced by the exhaust/external flow interaction processes at the trailing edge occur in mutually perpendicular planes. To best analyze the plume flowfield calculations in this vicinity, a combination of reference plane systems is employed. For the rectangular end module schematized in Fig. 7, vertical reference planes (y = constant) are employed in the central region while horizontal reference planes (z = constant) are used in the vicinity of the module sidewall. A cylindrical "wraparound" reference plane system is employed in the region of the corner to provide for the transition between these two systems. Implementation of this hybrid grid system provides reference plane alignment essentially perpendicular to predominant wave and discontinuity surfaces. While limited experience in performing such corner calculations has precluded defining an optimized approach for grid orientation in this region, it is found that the location of the origin of the cylindrical "wraparound" reference plane system cannot be fixed a priori in a generalized manner. Rather, the origin must be a "floating" one, which adjusts to the local growth rate of the plume interface both vertically and horizontally such as to best approximate the local radius of curvature in the "wraparound" region.

Multiple Module Interactions

In analyzing the plume interaction flowfield associated with exhausts emanating from multiple nozzles, the internal (nozzle) flowfield calculations are first performed for each individual module. The resultant exit plane properties may differ in pressure and stagnation properties from module to module. In addition, a discontinuity in cross-flow angle may exist produced by the finite trailing edge wedge angle in the common walls separating the individual modules. Thus, in addition to the primary interaction between the exhaust flow and external stream, a module-to-module interaction process occurs at the trailing edge of the walls separating adjacent modules, resulting in a wave system propagating predominantly in the spanwise direction. Preliminary results indicate the desirability of performing a localized detailed calculation at the intermodule wall trailing edge to establish "converged" starting conditions for the exhaust flow calculation. Since a finite number of integration steps are required to converge to the conically invariant solution whose boundary conditions are those associated with the flowfield in the immediate vicinity of the wedge/cowl trailing edge juncture, performing this calculation on a "large" grid scale (i.e., one commensurate with the remaining flow regions) can result in an influx of waves into this region before local convergence has been achieved.

Results

Two-Dimensional Convergent Duct

Calculations were performed for the duct geometry illustrated in Fig. 8 with $M = 2.94$ inlet conditions, employing a perfect gas option with $\gamma = 1.4$. The calculated shock propagation pattern obtained by BIGMAC is compared with the results of a two-dimensional floating shock code[12] (SEAGULL), interpreted to be nominally correct in this simple situation. The shock locations are quite good for the first few reflections, as are the pressure and entropy levels illustrated in Fig. 8 for the lower wall surface. Results of comparable quality have been obtained by CHAR3D.[9,10] The results obtained are particularly promising in view of the extremely coarse grid (11 points) employed. Results for the single wedge inlet presented in Refs. 7, 9, and 10 illustrate the gains achieved via grid refinement in a comparable situation. Results for a double-wedge inlet and divergent duct are reported in Refs. 9 and 10.

Internal Corners

Corner flowfields associated with interacting waves formed from mutually perpendicular surfaces represent ideal cases with which to test the developed codes. Experimental data and calculations exploiting the conical invariance of the reported cases are available for comparison. In these calculations, flow at the initial station was uniform and the interaction flowfield was generated by an abrupt change in wall angle at the initial station for the two mutually perpendicular surfaces. Results for an expansion-compression corner generated by an abrupt

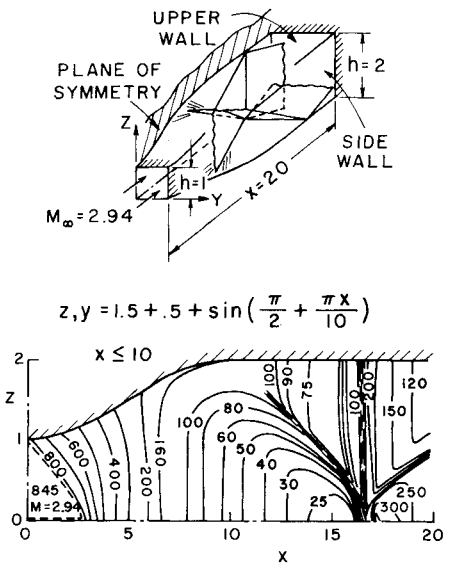

Fig. 10 Square nozzle calculation.

5-deg expansion and 7½-deg compression of a uniform Mach 2 flow are depicted in Fig. 9 as calculated by BIGMAC. An 11×11 Cartesian grid was employed and the results are depicted after 10 axial marching steps. These results are compared with the detailed conically invariant numerical solution of Shankar[13] and the experimental results of Nangia.[14] Further results for double-expansion and double-wedge compression corners, as calculated by CHAR3D and BIGMAC, are reported in Refs. 7, 9, and 10.

Square Nozzle

The three-dimensional flowfield within the square nozzle depicted in Fig. 10 has been calculated by BIGMAC. This flowfield is characterized by the initial interactions of expansion waves emanating from mutually perpendicular surfaces and the subsequent interaction of enveloping shock systems generated by recompression on the upper wall and sidewall. The initial Mach number was 2.94, and a perfect gas calculation with $\gamma = 1.4$ was performed. The calculation employed 21 grid points in each reference plane and 11 reference planes initially. Additional reference planes are automatically inserted as the module sidewall opens. The straight section here contained 18 reference planes. Calculated pressure contours are depicted on the symmetry plane ($y = 0$) and were virtually identical to those in the $z = 0$ plane, providing a check on the overall symmetry of the computational system. Similar checks with CHAR3D have not provided this required symmetry.

Single Module Nozzle-Exhaust Flowfield

The exhaust plume flowfield issuing from the single rectangular nozzle depicted in Fig. 11 was calculated by BIGMAC. The exhaust flow was assumed perfect ($\gamma = 1.4$) and had uniform conditions ($M = 1.7$, $P = 5.25$ psia, $T_t = 400°$F) at the combustor exit, while the external stream was quiescent ($P = 1.05$ psia, $T = 80°$F, $\gamma = 1.4$). The internal flowfield was two-dimensional and yielded an underexpanded flow situation along the cowl trailing edge and a mixed flow situation (partially overexpanded and partially underexpanded) along the end wall trailing edge. Resultant interface locations are depicted at several axial stations downstream of the cowl trailing edge station. To continue the calculation much beyond the last station, a relocation of the cylindrical origin would be required. This "floating origin" modification would appear requisite in all situations with some degree of overexpansion to account for the nonuniform collapse in plume size.

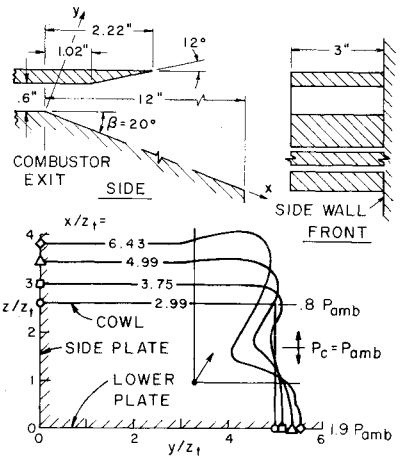

Fig. 11 Single module plume calculation.

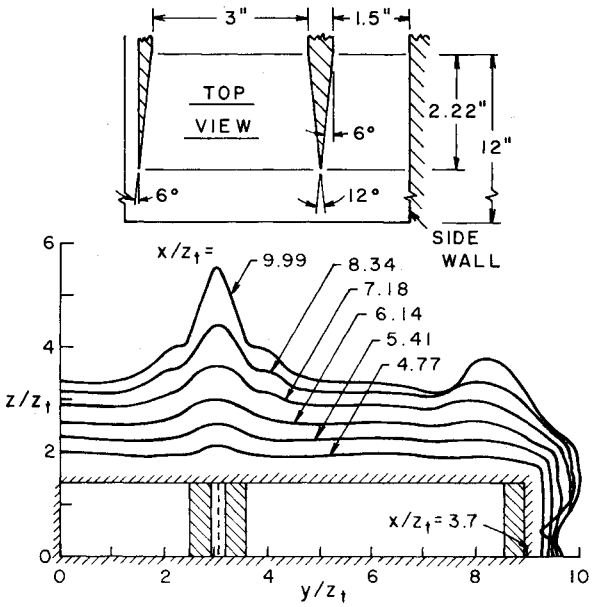

Fig. 12 Multiple module plume calculation.

Double Module Nozzle-Exhaust Flowfield

For this case, the side view is the same as that depicted in Fig. 11, while the top view is illustrated in Fig. 12. Initial conditions at the combustor exit are the same as for the single module case, but the external pressure of the quiescent stream is now .5 psia. Resultant interface locations at several axial stations are depicted, with qualitative support for the "peak" shape at the module juncture location provided by the results reported in Ref. 15 utilizing a floating shock procedure. It should be noted that the complete multiple nozzle and exhaust plume flowfield was calculated via one computer run, on a nonstop basis. BIGMAC calculated the internal flowfields for each of these modules employing a line source reference plane system up to the cowl trailing edge station, automatically interpolated the exit plane results for the two modules into a Cartesian framework, and then proceeded with the calculation of the multiple exhaust plume flowfield. The interaction processes at the trailing edges are all explicitly calculated, while the resultant cross-flow shocks are allowed to form numerically as the calculation evolves.

Conclusions

Preliminary applications of the BIGMAC and CHAR3D codes have demonstrated their capabilities in a variety of inviscid supersonic flow situations. The wave-preserving network in CHAR3D permits accurately tracing the propagation of shocks of modest strength within the reference

planes, but results in situations with strong wave systems propagating normal to the reference planes are inferior to those of BIGMAC. BIGMAC appears capable of producing nonpreferential results for generalized three-dimensional situations. Its ability to analyze complex flows with multiple shock interactions has been demonstrated, but a full assessment of its performance awaits the availability of further experimental data for such flows.

The applicability of BIGMAC is by no means limited to the prediction of nozzle-exhaust flowfields. With minor alterations, a version of BIGMAC (SUPFAN) has been developed to analyze the three-dimensional flow in a supersonic fan stage.[16] Modifications of BIGMAC to analyze viscous flow situations with finite-rate chemistry have been briefly discussed in Ref. 10. Such modifications would permit its analysis of the mixing processes along the plume interface and yield a more realistic representation of the nonequilibrium thermochemical processes occurring in the nozzle-exhaust flow.

Acknowledgments

This work was performed at Advanced Technology Laboratories, Inc., Westbury, N.Y., under contract NAS1-12726, monitored by M. Salas, LRC. The authors acknowledge the benefit of many fruitful discussions with the late A. Ferri in the preliminary development of these models and the assistance of P. Kalben in programming the computer codes.

References

[1] Moretti, G., Sanlorenzo, E. and Weilenstein, G., "Supersonic Flow About General Three-Dimensional Blunt Bodies," Flight Dynamics Laboratory, Aeronautical Systems Division, WPAFB, Ohio, ASD-TR-61-727, Vol. III, Oct. 1962.

[2] Katskova, O. N. and Chuskin, P. L., "Three-Dimensional Supersonic Equilibrium Flow of Gas Around Bodies at Angle of Attack," NASA TT F-9790, 1965.

[3] Rakich, J. V. and Cleary, J. W., "Theoretical and Experimental Study of Supersonic Steady Flow Around Inclined Bodies of Revolution," *AIAA Journal*, Vol. 8, March 1970, pp. 511-517.

[4] Dash, S. and DelGuidice, P., "Three-Dimensional Nozzle-Exhaust Flowfield Analysis by a Reference Plane Technique," AIAA Paper 72-704, Boston, Mass., June 1972.

[5] Dash, S., Del Guidice, P., Kalben, P., Ferri, A., and Roffe, G., "Analysis and Design of Three-Dimensional Supersonic Nozzles," Vol. I-IV, NASA CR 132350-132353, Oct. 1972.

[6] Rakich, J. V. and Kutler, P., "Comparison of Characteristics and Shock Capturing Methods with Application to the Space Shuttle Vehicle," AIAA Paper 72-191, San Diego, Calif., Jan. 1972.

[7] Dash, S. and DelGuidice, P., "Numerical Methods for the Calculation of Three-Dimensional Nozzle Exhaust Flowfields," *Aerodynamic Analyses Requiring Advanced Computers*, NASA SP-347, 1975, pp. 659-701.

[8] Dash, S. and Kalben, P., "Three-Dimensional Surface Representation and Interpolation Procedures Employing Cubic Spline Functions," Advanced Technology Laboratories, Westbury, N.Y., ATL TR 193, Jan. 1974.

[9] Dash, S. and DelGuidice, P., "Shock Capturing Finite-Difference and Characteristic Reference Plane Techniques for the Prediction of Three-Dimensional Nozzle-Exhaust Flowfields," Advanced Technology Laboratories, Westbury, N.Y., ATL TR 243, March 1977 (NASA CR in preparation).

[10] Dash, S. and DelGuidice, P., "Computational Models for the Analysis of Three-Dimensional Internal and Exhaust Plume Flowfields," *Proceedings of the JANNAF 10th Plume Technology Meeting*, Chemical Propulsion Information Agency Pub. 291, Vol. I, 1977, pp. 293-342.

[11] MacCormack, R. W., "The Effect of Viscosity in Hypervelocity Impact Cratering," AIAA Paper 69-354, Cincinnati, Ohio, 1969.

[12] Salas, M., "Shock Fitting Method for Complicated Two-Dimensional Supersonic Flows," *AIAA Journal*, Vol. 14, May 1976, pp. 583-588.

[13] Shankar, V. S. V., "Numerical Solutions for Inviscid Supersonic Corner Flows," AIAA Paper 75-221, Pasadena, Calif., Jan. 1975.

[14] Nangia, P. K., "Three-Dimensional Wave Interactions in Supersonic Intakes," 2nd International Symposium on Air Breathing Engines, Sheffield, England, March 1974.

[15] Rudman, S., "Multinozzle Plume Flowfields—Structure and Numerical Calculation," AIAA Paper 77-710, Albuquerque, N. Mex., June 1977.

[16] Ranlet, J., "Description of Fortran Program SUPFAN for the Analysis of the Steady, Inviscid Three-Dimensional Flow in a Supersonic Fan Stage," Advanced Technology Laboratories, Westbury, N.Y., ATL TM 199, April 1977.